

# Inference-Adaptive Neural Steering for Real-Time Area-Based Sound Source Separation

Martin Strauss, Wolfgang Mack, María Luis Valero and Okan Köpüklü

**Abstract**—We propose a novel *Neural Steering* technique that adapts the target area of a spatial-aware multi-microphone sound source separation algorithm during inference without the necessity of retraining the deep neural network (DNN). To achieve this, we first train a DNN aiming to retain speech within a target region, defined by an angular span, while suppressing sound sources stemming from other directions. Afterward, a phase shift is applied to the microphone signals, allowing us to shift the center of the target area during inference at negligible additional cost in computational complexity. Further, we show that the proposed approach performs well in a wide variety of acoustic scenarios, including several speakers inside and outside the target area and additional noise. More precisely, the proposed approach performs on par with DNNs trained explicitly for the steered target area in terms of DNSMOS and SI-SDR.

**Index Terms**—neural steering, real-time DNNs, source separation

## I. INTRODUCTION

THE modern workplace is shifting from traditional office settings to open-plan offices, hybrid work models, and fully remote employment. For 2022, the German Federal Statistics Office reports that 24.2% of employed people worked from home, with 14.7% doing so at least half the time, nearly doubling from pre-pandemic levels [1].

In this environment, virtual meetings are common, even in open offices, presenting challenges such as interfering speakers, background noise, and privacy concerns from recording non-participants.

A potential solution is to employ sound source separation techniques capable of separating the speech of meeting participants from all interfering sounds. Such an approach has two major requirements: (i) all speech utterances within a defined target spatial region should be kept to ensure all participants are covered and (ii) the employed solution should be real-time capable to prevent unwanted delays. Ideally, this target region is dynamically adaptable to other directions, allowing for the inclusion of more people and an intentional muting of individuals through steering away.

In this work, we present *Neural Steering*, an inference-based adaption of a sound source separating deep neural network (DNN) to new target regions. This is achieved by applying a phase shift to the audio captured by a microphone array. For

Martin Strauss is with the International Audio Laboratories (a joint institution of the Friedrich-Alexander-Universität Erlangen-Nürnberg and Fraunhofer IIS), 91058 Erlangen, Germany (e-mail: martin.strauss@audiolabs-erlangen.de). Wolfgang Mack is with Friedrich-Alexander-Universität Erlangen-Nürnberg email: wolfgang.mack@fau.de. María Luis Valero and Okan Köpüklü are with Microsoft Applied Sciences Group, Munich, Germany (email: okan.kopuklu@microsoft.com). Work done while the first author was doing an internship at Microsoft Applied Sciences Group.

this purpose, we first train a DNN architecture that preserves all speech utterances within a region-of-interest (ROI) only defined by an angular span w.r.t. the origin/center of a linear microphone array and suppresses speakers outside the ROI and noises. Afterward, applying the proposed approach can shift the ROI with negligible computational cost while keeping the DNN’s sound source separation ability.

The performance evaluation based on computational metrics shows that the proposed approach performs well in various settings, including multiple targets, interfering speakers, and noise.

## II. RELATED WORK

Source separation involves extracting individual audio sources from a mixture captured by one or more microphones. [2]. Multiple microphones enable the use of spatial filtering techniques, known as beamformers (BF), which utilize spatial information like time-difference-of-arrival [3] to enhance signals from a specific direction while suppressing others.

Traditional BF methods [4], [5], [6], [7], [8] are well-established but their performance relies on accurate signal modeling or direction of arrival estimation [9], [10].

With the advancements in DNNs, many combinations with BFs exist and enable non-linear spatial processing, e.g., used as a postfilter [11], [12] or standalone neural BFs [13], [14].

Recently, there’s been increasing interest in approaches that focus on the target signal’s location, based on a predefined region [15], [16], distance [17], [18], [19], or direction [19], [20]. These methods are often impractical for real-time applications due to computational complexity or the assumption of a single target speaker with a known source direction.

Our work builds on [21] and aims to efficiently steer a predefined ROI to other directions, while being independent from the specific location and number of speakers. In contrast to e.g. [13], no source direction is needed. Our scenario is conceptually similar to [22], but we use only a two-microphone setup and don’t rely on sampling the target direction.

## III. AREA-BASED SOUND SOURCE SEPARATION

For area-based sound source separation, the ROI is spanned by an angle  $\alpha$  in front of a microphone array with the center of the microphone array as origin. As the microphone array, we define a uniform linear array (ULA) with  $M \in \mathbb{N}^+$  microphones placed at random location in a room. Figure 1 (a) illustrates this setup for two microphones.

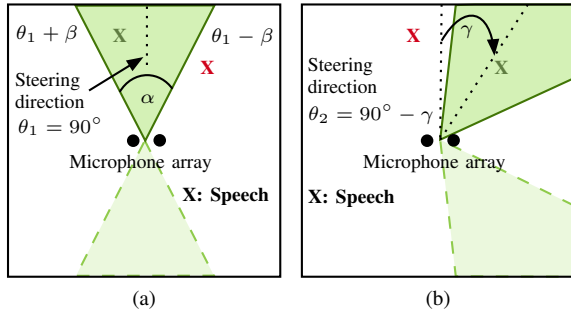


Fig. 1: Illustration of (a) the training setup for the area-based sound source separation and (b) applying Neural Steering to adapt the ROI to include the second speech source. Speech sources are denoted by **X** (Green: target, red: interferer). The ROI is defined by the angle  $\alpha$ . The dashed lines denote the mirrored area due to front-back ambiguity of the ULA.

The target signal spectrum  $\mathbf{X}_{t,m}(n, k)$  is determined by the summation of all speech signals inside the ROI in the short-time Fourier transform (STFT) domain, i.e.,

$$\mathbf{X}_{t,m}(n, k) = \sum_{r=1}^R \mathbf{X}_{t,m}^{(r)}(n, k), \quad (1)$$

where  $r \in [1, \dots, R]$  is the speaker index and  $n, k$  and  $m$  denote the time frame, frequency bin and microphone index.

Respectively, all interfering sources  $\mathbf{X}_{i,m}(n, k)$  are defined as the summed speech sources outside of the ROI, i.e.,

$$\mathbf{X}_{i,m}(n, k) = \sum_{l=1}^L \mathbf{X}_{i,m}^{(l)}(n, k), \quad (2)$$

with speaker index  $l \in [1, \dots, L]$ .

As a result, the STFT spectrum  $\mathbf{Y}_m(n, k)$  of an audio mixture captured by the microphones is expressed as the summation

$$\mathbf{Y}_m(n, k) = \mathbf{X}_{t,m}(n, k) + \mathbf{X}_{i,m}(n, k) + \mathbf{N}_m(n, k), \quad (3)$$

including all target and interfering signals, in addition to non-speech-like noise  $\mathbf{N}_m(n, k)$ . The noise can be located inside or outside the ROI.

The goal is to develop a DNN that learns to cover and extract signals from all active speech sources within the ROI. Therefore, it produces a separation mask  $Q \in \mathbb{C}^{N \times K \times 1}$  to separate the estimated target spectrum  $\hat{\mathbf{X}}_t(n, k)$  from the input signal by an element-wise complex multiplication, denoted by  $\odot$ , to the reference microphone signal  $\mathbf{Y}_{m=1}$ , i.e.,

$$\hat{\mathbf{X}}_t(n, k) = Q \odot \mathbf{Y}_{m=1}. \quad (4)$$

For this study we fix the number of microphones to be  $M = 2$  with the left microphone representing the reference.

#### IV. PROPOSED INFERENCE-ADAPTIVE NEURAL STEERING

Steering to new target areas typically requires multiple DNNs for different ROIs, which is computationally costly. Instead, we propose training for a single ROI and shifting

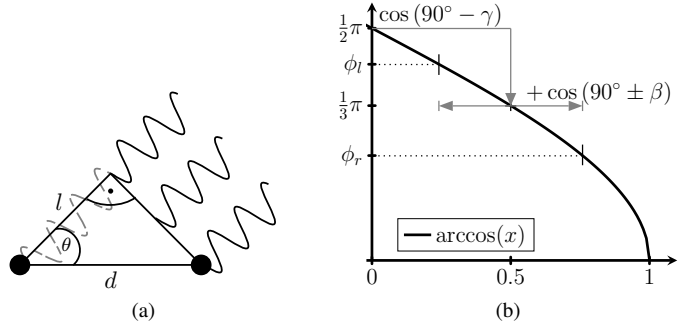


Fig. 2: In (a), a plane sound wave reaches the microphone array (incident angle  $\theta$ ). The dashed line symbolizes the phase shift caused by the extra travel distance  $l$  to the left microphone. (b) illustrates the arccos function to show the new ROI boundaries defined by the angles  $\phi_{l,r}$  after shifting the steering vector.

the entire ROI towards a new direction by applying a phase shift at inference time to the STFT spectrum of the second microphone. We term this approach *Neural Steering*, shown in Figure 1 (b).

To obtain the phase shift, we consider a far- and free-field scenario. The wave originating from a sound source reaches the microphones at different times [2]. Let  $d$  denote the distance between the two microphones and  $\theta$  the incident angle, then the distance  $l = d \cos(\theta)$  describes the additional way the incoming wave has to travel to the left microphone (see Figure 2(a)). This results in the inter-microphone phase difference  $\Delta\varphi_\theta = 2\pi f d \cos(\theta)/c$ , where  $f$  denotes the frequency and  $c$  the speed of sound.

Let the central line of the learned ROI be at  $\theta_1 = 90^\circ$  with respect to the microphone array.  $\theta_1$  denotes the initial steering direction of the trained DNN, with the inter-microphone phase difference  $\Delta\varphi_{\theta_1} = 0$ . As is illustrated in Figure 1 (b), we want to adapt  $\theta_1$  by an angle  $\gamma$ , defining a new steering direction denoted as  $\theta_2 = \theta_1 - \gamma$ , with phase difference  $\Delta\varphi_{\theta_2}$ .

Any signal reaching the microphone array at  $\theta_2$  must be adjusted with a phase shift  $\Delta\psi$  so that it appears to the DNN to originate from  $\theta_1$ , i.e.,

$$\Delta\varphi_{\theta_1} = \Delta\varphi_{\theta_2} + \Delta\psi \quad (5)$$

where  $\Delta\psi = 2\pi f \frac{d}{c} (\cos(\theta_1) - \cos(\theta_2))$ . This effectively simulates to the network that the signals in the steered area are located within the initially learned ROI.

The adapted spectrum  $\tilde{\mathbf{Y}}_{m=2}$  is obtained by multiplying the STFT representation of the second microphone with a vector  $\mathbf{a} \in \mathbb{C}^K$ , with  $K$  denoting the number of frequency bins, i.e.,

$$\mathbf{a}(k) = e^{j\Delta\psi} \stackrel{\theta_1=90^\circ}{=} e^{-j2\pi f \frac{d}{c} \cos \theta_2}. \quad (6)$$

$$\tilde{\mathbf{Y}}_{m=2}(n, k) = \mathbf{a}(k) \mathbf{Y}_{m=2}(n, k). \quad (7)$$

As is shown in Figure 1 (a), the initial ROI boundaries are defined by an angular width  $\beta$ . Then,  $\Delta\varphi_l$  and  $\Delta\varphi_r$  denote the

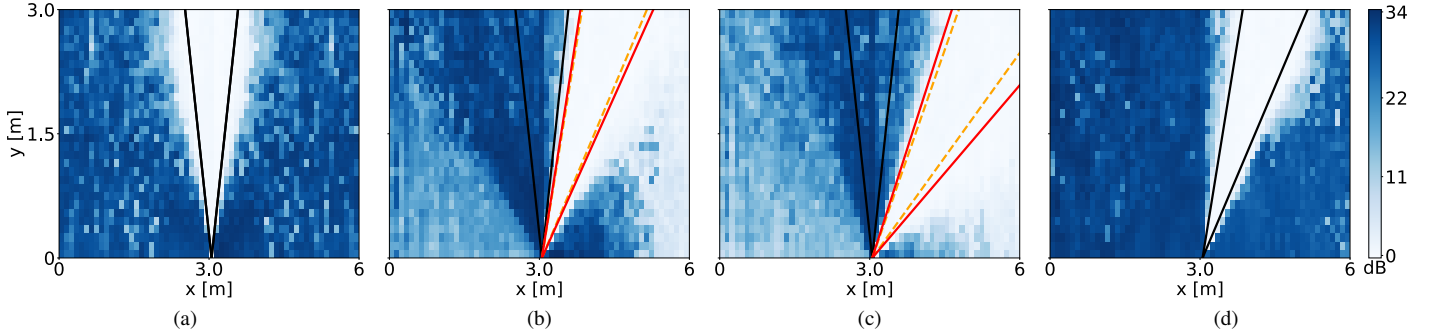


Fig. 3: PR heatmaps of the trained CRUSE<sub>20</sub> model when (a) no steering, (b) clockwise steering of 25° and (c) 40° is applied. (d) shows the baseline model CRUSE<sub>b-20</sub> that was trained to cover the ROI at a steered angle of 25°. The darker regions show stronger signal suppression. Black lines mark the original ROI, dashed orange lines mark the steered ROIs for completely linear steering, and solid red lines show the adapted ROI based on Equation 11. Due to front-back ambiguity, only one half of the room is shown.

phase differences present at the left and right ROI boundaries, defined as  $\Delta\varphi_{l,r} = 2\pi f \frac{d}{c} \cos(\theta_1 \pm \beta)$ .

The corresponding phase differences  $\Delta\varphi_{\phi_{l,r}}$  of the shifted ROI boundaries are now characterized by the angles  $\phi_{l,r}$ , i.e.,

$$\Delta\varphi_{\phi_{l,r}} = 2\pi f \frac{d}{c} \cos(\phi_{l,r}). \quad (8)$$

The phase differences at the initial ROI boundaries can then be expressed as  $\Delta\varphi_{l,r} = \Delta\varphi_{\phi_{l,r}} + \Delta\psi$ . Using  $\Delta\varphi_{l,r}$ , Equation 5 and solving for  $\phi_{l,r}$  results in

$$2\pi f \frac{d}{c} \cos(\theta_1 \pm \beta) = 2\pi f \frac{d}{c} \cos(\phi_{l,r}) + 2\pi f \frac{d}{c} (\cos(\theta_1) - \cos(\theta_2)). \quad (9)$$

$$\cos(\theta_1 \pm \beta) = \cos(\phi_{l,r}) + 0 - \cos(\theta_1 - \gamma). \quad (10)$$

$$\phi_{l,r} = \arccos(\cos(\theta_1 \pm \beta) + \cos(\theta_1 - \gamma)). \quad (11)$$

Two observations can be made here: (i) steering the ROI is frequency independent, and (ii) the dependency of  $\phi$  on the arccos function leads to a non-linear change in the shifted ROI boundaries, increasing the overall area. Figure 2 (b) illustrates this for  $\beta = 15^\circ$  and  $\gamma = 30^\circ$ .

## V. EXPERIMENTAL SETUP

### A. Model architecture

We used the CRUSE model [23] for this work. It is a real-time capable U-Net architecture [24] operating in the STFT domain. As input, we concatenated the STFT representation of the stereo input along the channel dimension. Trained models generate a complex-valued single-channel separation mask, which was applied to the left channel of the input spectrum. Training used the AdamW optimizer [25] with a 0.001 learning rate,  $2e-05$  weight decay, and the SI-SDR [26] as a loss function. The STFT computation used a 20 ms square-root Hann window (50% overlap) and 320 NFFT points.

Overall, the model had approximately 640k parameters with 9.18 GFLOPS in terms of computational complexity. A real-time factor (RTF) of 0.04 was obtained by computing the

average processing time of 100 files of 10 s length on a laptop with an 11th Gen. Intel(R) Core(TM) i7-1185G7 @ 3.00GHz.

### B. Training dataset

A synthetic dataset was created using the pyroomacoustics package [27] to simulate the scenario. A two-microphone ULA was placed randomly in a shoebox room, with at least 2 m distance to each wall. The room dimensions were uniformly sampled at [4.0 m × 4.0 m × 2.0 m] to [8.0 m × 8.0 m × 4.0 m] with T60 values randomly chosen from 0.25 to 0.7 s to mimic an office-like scenario [2]. The microphone array and sources were assumed to be at the same height. Disjoint sets of speech and noise utterances from the DNS-Challenge dataset [28] at 16 kHz were used for training. No sources were placed in the array's mirrored ROI to avoid front-back ambiguity.

Each generated clip was 10 s long and included one target and one interfering speaker, mixed at a signal-to-interference ratio (SIR) uniformly sampled between 0 and 10 dB. Noise was added to the mix with SNR values that were sampled from a Gaussian  $\mathcal{N}(7, 3)$  distribution. The mix was level normalized using values from  $\mathcal{N}(-28, 10)$  dBFS, generating 55.6 h of training data.

To understand how ROI size affects separation and steering performance, we trained two model versions, CRUSE<sub>20</sub> and CRUSE<sub>40</sub>, with target area angles  $\alpha = \{20^\circ, 40^\circ\}$ . Both models used the same configuration but separate training sets.

### C. Test setup

For CRUSE<sub>20</sub> and CRUSE<sub>40</sub> models, we generated separate test sets with the ROI steered 25° and 45° clockwise, respectively. Using speech from the 2020 Interspeech DNS-challenge [29] test set and noise from FSDnoisy18k [30], each test set included 4 scenarios varying the number of target and interfering speakers, with or without additional noise sources. Target sources were placed within the steered ROIs, and interfering sources remained in the initial ROI. This way it can be demonstrated that we can also mute the originally learned ROI using the proposed steering. Each test scenario included 100 clips.

TABLE I: DNSMOS and SI-SDR results (mean $\pm$ std) for the test scenarios with different number of speakers and with/without noise.  $t$  and  $k$  represent target and interfering speech sources respectively. 1 denotes that a single source was present, whereas 23 represent randomly sampled 2 or 3 speakers.

Steering Angle	Method	Noise	$\Delta$ SIG		$\Delta$ BAK		$\Delta$ OVRL		$\Delta$ SI-SDR	
			$t1$ k1	$t23$ k23	$t1$ k1	$t23$ k23	$t1$ k1	$t23$ k23	$t1$ k1	$t23$ k23
$25^\circ$	CRUSE <sub>b-20</sub>	✓	<b>0.16</b> $\pm$ 0.60	<b>0.99</b> $\pm$ 0.49	$1.53$ $\pm$ 0.53	<b>1.65</b> $\pm$ 0.41	<b>0.68</b> $\pm$ 0.34	<b>0.73</b> $\pm$ 0.27	$7.20$ $\pm$ 2.52	$2.98$ $\pm$ 2.61
	CRUSE <sub>20</sub>	✓	$0.12$ $\pm$ 0.60	$0.94$ $\pm$ 0.52	<b>1.60</b> $\pm$ 0.51	$1.53$ $\pm$ 0.52	<b>0.68</b> $\pm$ 0.34	$0.67$ $\pm$ 0.32	<b>7.42</b> $\pm$ 2.68	<b>3.16</b> $\pm$ 2.65
$45^\circ$	CRUSE <sub>b-40</sub>	✓	<b>0.38</b> $\pm$ 0.77	<b>1.08</b> $\pm$ 0.53	<b>1.70</b> $\pm$ 0.63	<b>1.70</b> $\pm$ 0.52	<b>0.78</b> $\pm$ 0.47	<b>0.80</b> $\pm$ 0.36	<b>7.66</b> $\pm$ 2.20	$3.18$ $\pm$ 3.33
	CRUSE <sub>40</sub>	✓	$0.36$ $\pm$ 0.76	$1.07$ $\pm$ 0.56	$1.66$ $\pm$ 0.59	$1.57$ $\pm$ 0.54	$0.76$ $\pm$ 0.45	$0.74$ $\pm$ 0.36	$7.32$ $\pm$ 2.68	<b>3.55</b> $\pm$ 2.97
$25^\circ$	CRUSE <sub>b-20</sub>	✗	<b>-0.05</b> $\pm$ 0.53	$0.95$ $\pm$ 0.60	$1.27$ $\pm$ 0.53	<b>1.67</b> $\pm$ 0.49	$0.50$ $\pm$ 0.41	<b>0.76</b> $\pm$ 0.36	<b>6.35</b> $\pm$ 2.03	$0.93$ $\pm$ 3.05
	CRUSE <sub>20</sub>	✗	$-0.07$ $\pm$ 0.51	<b>0.98</b> $\pm$ 0.60	<b>1.34</b> $\pm$ 0.55	$1.62$ $\pm$ 0.50	<b>0.52</b> $\pm$ 0.42	$0.74$ $\pm$ 0.37	$6.16$ $\pm$ 2.58	<b>1.04</b> $\pm$ 3.09
$45^\circ$	CRUSE <sub>b-40</sub>	✗	<b>0.08</b> $\pm$ 0.57	<b>1.06</b> $\pm$ 0.52	$1.35$ $\pm$ 0.59	<b>1.74</b> $\pm$ 0.39	<b>0.62</b> $\pm$ 0.43	<b>0.81</b> $\pm$ 0.32	<b>7.30</b> $\pm$ 2.21	$1.47$ $\pm$ 3.33
	CRUSE <sub>40</sub>	✗	$0.04$ $\pm$ 0.57	<b>1.06</b> $\pm$ 0.51	<b>1.37</b> $\pm$ 0.56	$1.59$ $\pm$ 0.50	$0.60$ $\pm$ 0.42	$0.76$ $\pm$ 0.31	$6.72$ $\pm$ 2.50	<b>1.56</b> $\pm$ 2.92

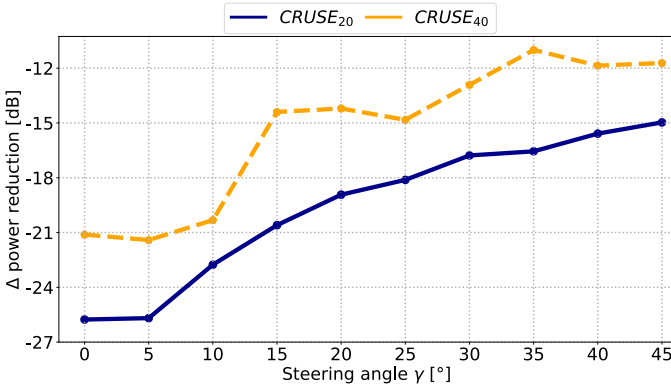


Fig. 4: PR performance of CRUSE $_{\{20,40\}}$  models at different steering angles.  $\Delta$ PR is computed as the difference of mean PR in the ROI and the area outside.

As baseline methods two models termed CRUSE<sub>b-20</sub> and CRUSE<sub>b-40</sub> were trained to specifically cover the steered ROI without the proposed phase shift.

#### D. Performance Evaluation

We use power reduction (PR) heatmaps to visualize the effectiveness of our approach. Therefore, a single speech utterance is placed along the x and y direction in a room of size [6 m  $\times$  6 m  $\times$  3 m], with a  $T60 = 0.5$  s. At each position, the PR metric [18] is computed by

$$PR_{dB} := 10 \log_{10} (||\mathbf{y}_{m=1}||^2 / ||\hat{\mathbf{t}}||^2), \quad (12)$$

where  $\mathbf{y}_{m=1}$  and  $\hat{\mathbf{t}}$  are the time domain representations of the mixture input signal at the reference microphone and the estimated target signal, respectively. Ideally, the PR should be strong outside the ROI and show no reduction inside. This setup enables us to create heatmaps to visualize the model's coverage of the ROI and its changes after steering.

In addition, we report the DNSMOS [31] and SI-SDR [26] as evaluation metrics. DNSMOS is composed of sub-metrics evaluating the signal quality (SIG), background (BAK), and overall quality (OVRL). SI-SDR is the metric on which all models were optimized. The improvement ( $\Delta$ ) compared to the input mixture signal is reported for all metrics.

## VI. RESULTS AND DISCUSSION

We first investigated the *Neural Steering* performance with PR heatmaps in Figure 3. The heatmaps were generated using the CRUSE<sub>20</sub> model for steering angles of  $0^\circ$  (i.e., no steering),  $25^\circ$  and  $45^\circ$ . In addition, the heatmap of the corresponding baseline model is shown. This analysis demonstrates that *Neural Steering* can successfully steer the ROI in new directions.

Second, we investigated the performance of *Neural Steering* for different steering angles in Figure 4. The figure shows the difference of mean PR of all positions within the ROI and the area outside against the steering angles for the CRUSE $_{\{20,40\}}$  models. The steering was evaluated in five degrees steps until  $45^\circ$ . We observe that the PR is the strongest for the initial learned ROI at  $\gamma = 0$  and decreases with increasing steering values. This demonstrates that with increasing steering angles the non-linear mapping of the ROI also leads to less suppression close to the ROI boundaries. This effect can also be found in Figure 3, where the brighter area indicating low suppression increases with an increasing steering angle. Notably, the precision of the steered ROI decreases as the sources move further from the microphone array and the steering angle increases.

Lastly, we investigated the performance of *Neural Steering* in terms of DNSMOS and SI-SDR compared to the baseline approaches in Table I. For this analysis, we investigated the CRUSE<sub>20</sub>, CRUSE<sub>40</sub> models' performance for steering angles of  $25^\circ$  and  $45^\circ$ . The baseline models are trained with their respective ROI at these angles.

In general, all approaches show better improvements in '*with noise*' scenarios compared to '*without noise*', indicating their capability to suppress noise. Overall, the proposed *Neural Steering* approach on CRUSE models shows comparable results to baselines in all scenarios. This demonstrates that our approach can steer to new target directions at negligible cost, reinforcing its practicality without the need for retraining the DNN for each direction.

## VII. CONCLUSION

This work proposed *Neural Steering*, an inference-adaptive steering method for real-time audio source separation. This is achieved by applying a phase shift to the captured audio, which steers a trained DNN to a new target area, including the desired

speech utterances. In the future, we intend to combine this approach with a direction-of-arrival estimator to track moving target speakers such that steering can be applied dynamically over time.

## REFERENCES

- [1] “German Federal Statistics Office, “Quality of Employment - Employed persons working from home”,” [https://www.destatis.de/EN/Themes/Labour/Labour-Market/Quality-Employment/Dimension3/3\\_11\\_homeoffice.html](https://www.destatis.de/EN/Themes/Labour/Labour-Market/Quality-Employment/Dimension3/3_11_homeoffice.html), [Online] Accessed: 2024-04-12.
- [2] E. Vincent, S. Gannot, and T. Virtanen, *Acoustics: Spatial Properties*. John Wiley and Sons, Ltd, 2018, ch. 3, pp. 31–45.
- [3] J. Benesty, J. Chen, and Y. Huang, “Conventional beamforming techniques,” in *Microphone Array Signal Processing*. Springer Berlin Heidelberg, 2008, pp. 39–65.
- [4] V. Perrot, M. Polichetti, F. Varray, and D. Garcia, “So you think you can DAS? A viewpoint on delay-and-sum beamforming,” *Ultrasonics*, vol. 111, p. 106309, 2021.
- [5] L. Griffiths and C. Jim, “An alternative approach to linearly constrained adaptive beamforming,” *IEEE Transactions on Antennas and Propagation*, vol. 30, no. 1, pp. 27–34, 1982.
- [6] J. Zhang and C. Liu, “On Linearly Constrained Minimum Variance Beamforming,” *Journal of Machine Learning Research*, vol. 16, no. 1, pp. 2099–2145, 2015.
- [7] M. Souden, J. Benesty, and S. Affes, “On optimal frequency-domain multichannel linear filtering for noise reduction,” *IEEE Transactions on Audio, Speech, and Language Processing*, vol. 18, no. 2, pp. 260–276, 2009.
- [8] T. Lotter and P. Vary, “Dual-channel speech enhancement by superdirective beamforming,” *EURASIP Journal on Advances in Signal Processing*, vol. 2006, pp. 1–14, 2006.
- [9] S. Chakrabarty and E. A. P. Habets, “Multi-Speaker DOA Estimation Using Deep Convolutional Networks Trained With Noise Signals,” *IEEE Journal of Selected Topics in Signal Processing*, vol. 13, no. 1, pp. 8–21, 2019.
- [10] M. Taseska and E. A. P. Habets, “DOA-informed source extraction in the presence of competing talkers and background noise,” *EURASIP J. Adv. Signal Process.*, vol. 60, 2017.
- [11] K. Tesch and T. Gerkmann, “Insights Into Deep Non-Linear Filters for Improved Multi-Channel Speech Enhancement,” *IEEE/ACM Transactions on Audio, Speech, Language Processing*, vol. 31, pp. 563–575, 2023.
- [12] Y. Yang, S.-F. Shih, H. Erdogan, J. Menjay Lin, C. Lee, Y. Li, G. Sung, and M. Grundmann, “Guided Speech Enhancement Network,” in *Proc. IEEE Intl. Conf. on Acoustics, Speech and Signal Processing (ICASSP)*, 2023, pp. 1–5.
- [13] K. Tesch and T. Gerkmann, “Multi-Channel Speech Separation Using Spatially Selective Deep Non-Linear Filters,” *IEEE/ACM Transactions on Audio, Speech, and Language Processing*, vol. 32, pp. 542–553, 2024.
- [14] R. Liu, Y. Zhou, H. Liu, X. Xu, J. Jia, and B. Chen, “A New Neural Beamformer for Multi-channel Speech Separation,” *Journal of Signal Processing Systems*, vol. 94, no. 10, pp. 977–987, 2022.
- [15] A. Xu and R. R. Choudhury, “Learning to Separate Voices by Spatial Regions,” in *Proceedings of the 39th International Conference on Machine Learning*, vol. 162. PMLR, 17–23 Jul 2022, pp. 24539–24549.
- [16] J. Wechsler, S. R. Chetupalli, W. Mack, and E. A. P. Habets, “Multi-Microphone Speaker Separation by Spatial Regions,” in *Proc. IEEE Intl. Conf. on Acoustics, Speech and Signal Processing (ICASSP)*, 2023, pp. 1–5.
- [17] M. Yiwere and E. J. Rhee, “Sound Source Distance Estimation Using Deep Learning: An Image Classification Approach,” *IEEE Sensors J.*, vol. 20, no. 1, p. E172, December 2019.
- [18] K. Patterson, K. Wilson, S. Wisdom, and J. R. Hershey, “Distance-Based Sound Separation,” in *Proc. Interspeech Conf.*, 2022, pp. 901–905.
- [19] H. Taherian, K. Tan, and D. Wang, “Multi-Channel Talker-Independent Speaker Separation Through Location-Based Training,” *IEEE/ACM Transactions on Audio, Speech, Language Processing*, vol. 30, pp. 2791–2800, 2022.
- [20] T. Jenrungrat, V. Jayaram, S. Seitz, and I. Kemelmacher-Shlizerman, “The Cone of Silence: Speech Separation by Localization,” in *Advances in Neural Information Processing Systems*, vol. 33, 2020, pp. 20925–20938.
- [21] M. Strauss and O. Köpüklü, “Efficient area-based and speaker-agnostic source separation,” in *International Workshop on Acoustic Signal Enhancement (IWAENC) (to appear)*, 2024, available at <https://arxiv.org/abs/2408.09810>.
- [22] R. Gu and Y. Luo, “ReZero: Region-customizable Sound Extraction,” *IEEE/ACM Trans. Audio, Speech, Lang. Process.*, pp. 1–14, 2024.
- [23] S. Braun, H. Gamper, C. K. Reddy, and I. Tashev, “Towards Efficient Models for Real-Time Deep Noise Suppression,” in *Proc. IEEE Intl.*

*Conf. on Acoustics, Speech and Signal Processing (ICASSP)*, 2021, pp. 656–660.

[24] P. F. O. Ronneberger and T. Brox, “U-Net: Convolutional Networks for Biomedical Image Segmentation,” in *Medical Image Computing and Computer-Assisted Intervention—MICCAI*, 2015, pp. 234—241.

[25] I. Loshchilov and F. Hutter, “Decoupled Weight Decay Regularization,” in *International Conference on Learning Representations*, 2018.

[26] J. L. Roux, S. Wisdom, H. Erdogan, and J. R. Hershey, “SDR – Half-baked or Well Done?” in *Proc. IEEE Int. Conf. on Acoustics, Speech and Signal Processing (ICASSP)*, 2019, pp. 626–630.

[27] R. Scheibler, E. Bezzam, and I. Dokmanić, “Pyroomacoustics: A Python Package for Audio Room Simulation and Array Processing Algorithms,” in *Proc. IEEE Int. Conf. on Acoustics, Speech and Signal Processing (ICASSP)*, 2018, pp. 351–355.

[28] H. Dubey, A. Aazami, V. Gopal, B. Naderi, S. Braun, R. Cutler, A. Ju, M. Zohourian, M. Tang, H. Gamper, M. Golestaneh, and R. Aichner, “Deep speech enhancement challenge at icassp 2023,” in *Proc. IEEE Int. Conf. on Acoustics, Speech and Signal Processing (ICASSP)*, 2023.

[29] C. K. A. Reddy, V. Gopal, R. Cutler, E. Beyrami, R. Cheng, H. Dubey, S. Matusevych, R. Aichner, A. Aazami, S. Braun, P. Rana, S. Srinivasan, and J. Gehrke, “The INTERSPEECH 2020 Deep Noise Suppression Challenge: Datasets, Subjective Testing Framework, and Challenge Results,” in *Proc. Interspeech Conf.*, 2020, pp. 2492–2496.

[30] E. Fonseca, M. Plakal, D. P. W. Ellis, F. Font, X. Favory, and X. Serra, “Learning Sound Event Classifiers from Web Audio with Noisy Labels,” in *Proc. IEEE Int. Conf. on Acoustics, Speech and Signal Processing (ICASSP)*, 2019, pp. 21–25.

[31] C. K. A. Reddy, H. Dubey, V. Gopal, R. Cutler, S. Braun, H. Gamper, R. Aichner, and S. Srinivasan, “ICASSP 2021 Deep Noise Suppression Challenge,” in *Proc. IEEE Int. Conf. on Acoustics, Speech and Signal Processing (ICASSP)*, 2021, pp. 6623–6627.